Engineering Failure Analysis 111 (2020) 104451

Contents lists available at ScienceDirect

Engineering Failure Analysis

journal homepage: www.elsevier.com/locate/engfailanal

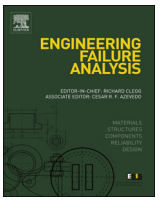

Mechanical properties and phases evolution in T91 steel during long-term high-temperature exposure

Yuyang Li[a,b], Jinfeng Du[c], Linping Li[c], Kewei Gao[a,b], Xiaolu Pang[a,b,*], Alex A. Volinsky[d]

[a] Beijing Advanced Innovation Center for Materials Genome Engineering, Beijing 100083, China
[b] School of Materials Science and Engineering, University of Science and Technology Beijing, Beijing 100083, China
[c] Shenhua Guohua (Beijing) Electric Power Research Institute Co., Ltd., Beijing 100025, China
[d] Department of Mechanical Engineering, University of South Florida, Tampa, FL 33620, USA

ARTICLE INFO

Keywords:
T91 steel
Long-team service
Microstructure
Mechanical properties
Electrochemical tests

ABSTRACT

Scanning and transmission electron microscopy was used to characterize quantity, pattern, size, and distribution of microstructure and precipitated phases in T91 steel exposed to high temperature in the subcritical unit superheater of a specific power plant. The materials were mechanically and electrochemically tested using a universal testing machine and an electrochemical workstation. The structure and performance of the original material and after the long-term service time were compared. The hardness and strength of T91 steel initially increased before they decreased during long-term service. It took 4000 h for the T91 steel to transform from the original to the service state, forming $(Cr, Fe, V, Mo)_{23}C_6$ multi-component mixed phase, which delayed or inhibited the growth of the $M_{23}C_6$-type carbides during the long-term high-temperature service. The MX-type carbide formation would pin dislocations and increase the strength. When the service time was between 4000 and 130,000 h, the carbide coarsening was obvious, and the effect of solid solution strengthening was reduced, the dislocation density was decreased, reducing the material's strength below the original state level. Electrochemical tests showed that longer service time degraded corrosion resistance of the T91 steel.

1. Introduction

T91 steel is the new 9Cr-1Mo steel developed by the Oak Ridge National Laboratory in the 1970s [1,2]. It has strong corrosion resistance, steam oxidation resistance, and good creep rupture strength. The strength at 625 ˚C is comparable to the TP304H steel, and the T91 steel has good thermal conductivity and low coefficient of thermal expansion. Therefore, it is an ideal material for manufacturing superheaters, reheaters and main steam chambers of power station boilers. T91 steel has been widely used in large-capacity and high-efficiency subcritical and supercritical units of new and in-service power plants worldwide [3–7].

Although heat-resistant steel is widely used in high-temperature and high-pressure steam lines and other high-temperature components in thermal power plants, materials degradation, failure, and corrosion are inevitable due to the long-term high-temperature exposure, high pressure, and other harsh environmental conditions. In addition, due to aerobic service conditions, materials' corrosion can't be ignored [8]. Failures after long-term operation of superheater pipelines and main steam pipelines are the major

* Corresponding author at: Beijing Advanced Innovation Center for Materials Genome Engineering, School of Materials Science and Engineering, University of Science and Technology Beijing, Beijing 100083, China (X. Pang).
E-mail address: pangxl@mater.ustb.edu.cn (X. Pang).

https://doi.org/10.1016/j.engfailanal.2020.104451
Received 2 September 2019; Received in revised form 10 February 2020; Accepted 13 February 2020
Available online 19 February 2020
1350-6307/

Table 1
T91 chemical composition in wt.%.

Sample	C	Si	Mn	Cr	Mo	V	Ni	Al	Nb	P	S
Original	0.1	0.27	0.42	8.74	0.96	0.21	0.073	0.015	0.105	0.003	0.004
ASME standard	0.07–0.14	0.2–0.5	0.3–0.6	8–9.5	0.85–1.05	0.18–0.25	≤0.4	≤0.02	0.06–0.1	≤0.02	≤0.01

factors affecting boiler safety and operation. Safety of the whole power plant depends on the pipelines' safe and stable operation. T91 steel has been operating at high temperatures and pressures for a long time in many power plant applications. Increased service time results in material aging, causing mechanical properties degradation [9–13].

The precipitated phases affect mechanical behavior of T91 steel, including fracture modes and creep deformation [14,15]. The volume and size of precipitated particles are affected by the service temperature and time. At present, most researchers focus on the changes in microstructure and properties of T91 steel after short or medium service time, and only a few reports focus on materials operating over long service time. Pandey et al. [16,17] investigated microstructure, precipitated phases and mechanical properties of P91 steels after 4000 h at 650 °C aging, which demonstrated the effects of precipitated phases on mechanical properties, but the samples didn't serve in a power plant. Thus, there is a need to study mechanical properties and microstructure of the actual ultra-long service T91 steel pipes. Therefore, this paper investigates the microstructure, mechanical properties, and electrochemistry of T91 steel used for 4000 and 130,000 h in a power plant. The microstructure, precipitation phase distribution, mechanical properties and corrosion resistance of the T91 steel during service were observed. Predicting the aging state of the material in advance provides data for the evaluation of the T91 steel lifetime.

2. Experimental procedure

The test material is T91 steel from the superheater pipeline operated at 545 °C and 18.2 MPa for a different time in a power plant in Zhuhai, China. The chemical composition is listed in Table 1. It can be seen from Table 1 that the chemical composition of T91 steel meets the standard [18].

Microstructure analysis was performed using a Zeiss Auriga focused ion beam field emission scanning electron microscope. The T91 steel sample was polished from 60 to 5000 grit, and the diamond particle polishing agent was used. After acetone degreasing, the sample was etched with a mixture of 5 g $FeCl_3$ + 50 ml hydrochloric acid + 100 ml deionized water solution. The spectrometer was used to analyze the morphology and composition of the precipitated phases. The working voltage was 15 kV and the working distance was 10 mm. At the same time, three sets of samples with different service durations were observed at 10,000× magnification multiple times by scanning electron microscopy. For each group 10 images were randomly taken and analyzed by the Image-Pro Plus software to count the size of the precipitated phase in the image and the percentage of the precipitated area, recording the average value.

Microstructure analysis was performed using the Technai F-20 field emission transmission electron microscope. First, the TEM samples were polished to less than 80 μm thickness, and then a circular sample with a diameter of 3 mm was punched out. Then the samples were prepared by twin-jet polishing in the solution of 5 vol.% perchloric acid and 95 vol% ethanol at 30 V voltage and −30 °C temperature.

The hardness of the T91 steel was tested using the EM1500L Vickers hardness tester with a load of 100 g and a loading time of 10 sec. Each sample was measured ten times, averaged and recorded. The tensile tests were carried out using the UTM5105 universal

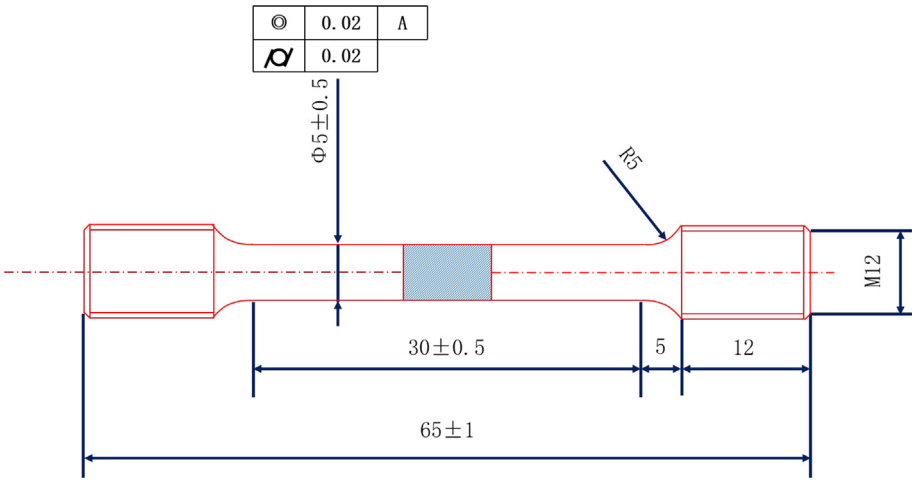

Fig. 1. The shape and size of the tensile specimen. Dimensions are in mm.

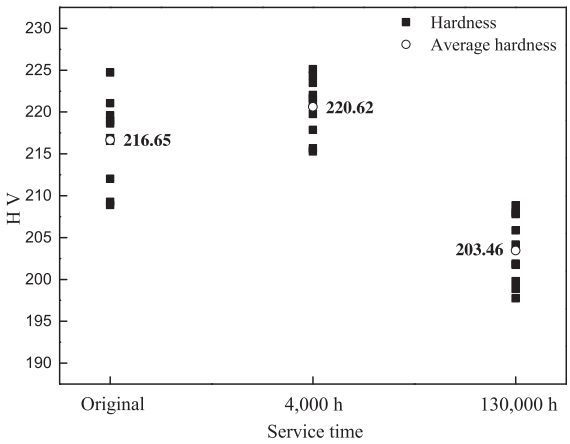

Fig. 2. The average hardness of the T91 steel after different service time.

testing machine at room temperature, 0.00025 s^{-1} strain rate, three samples were tested, and the average value was recorded. The shape and dimensions of the tensile specimen are shown in Fig. 1.

The potentiometric polarization tests were performed using the CS310 electrochemical workstation. The sample was cut into 10 mm × 10 mm × 3 mm size and sealed with an epoxy resin to expose the 1 cm^2 working surface, and a gap between the epoxy resin and the sample was sealed with silicone to avoid crevice corrosion. Before the test, the working electrode was sanded with 800 grit paper, and the sample was ultrasonically degreased in acetone after washing with deionized water. The sample, the platinum plate, and the saturated calomel electrode were respectively used as the working electrode, the auxiliary electrode, and the reference electrode to form a three-electrode system, and the electrochemical test conditions were room temperature and 3.5 wt% sodium chloride solution. First, the sample was measured in the open circuit potential (OCP) for at least one hour, then the system stabilized, and the potentiodynamic scan was performed. The scanning interval of the polarization potential was −0.3–0.5 V vs. OCP, and the scan rate was 0.5 mV/s. The polarization curves were fitted with the CView2 software that came with the electrochemical workstation.

3. Results and discussion

3.1. Vickers hardness measurements

Changes in the hardness reflect the changes in the microstructure of the T91 steel during aging. Fig. 2 shows that the hardness of the original state T91 steel is 216.65 HV, and the hardness after 4000 h of service is 220.62 HV, while the hardness after 130,000 h of service is 203.46 HV, and it first increases and then decreases with service time. The size, amount, and distribution of the precipitates and microstructure changes will affect the hardness [15,19]. As the service time increases, the precipitated phase is continuously precipitated first, resulting in precipitation strengthening, and the hardness increase. At longer service time, the carbide coarsening is serious, the depletion phenomenon of the solid solution alloy elements is severe, resulting in decreased hardness. Coarsening of $M_{23}C_6$ carbide will cause hardness reduction.

3.2. Tensile tests

Fig. 3 shows the stress-strain curves of the T91 steel in the original state, and after 4000 h and 130,000 h in service. σ_{TS}, σ_{YS}, δ, and Ψ represent the tensile strength, yield strength, elongation and reduction of area, respectively. The reduction of the area was 53%, 44%, and 49%, respectively, and the elongation was 28%, 24%, and 29%, respectively. The overall change was not large, since the original states were σ_{TS} 675 MPa and σ_{YS} 542 MPa, while after 4000 h in service σ_{TS} was 714 MPa and σ_{YS} was 545 MPa, which increased by 6% and 0.6% compared with the original state. When the service life was 130,000 h, the numbers changed to σ_{TS} 642 MPa and σ_{YS} 479 MPa, which is 5% and 11.6% lower than the original state. It is worth noting that the tensile strength and yield strength of the T91 steel increased first and then decreased with the service time, which correlates with the hardness results. In order to study the reasons for this change, the microstructure was further analyzed.

Fig. 4 shows the SEM fracture morphology after tensile testing. Fig. 4(a, c, e) show fracture surfaces at low magnification, where distinctive radial cracks are visible. This form of cracking is commonly called “splitting” [14]. Fig. 4(b, d, f) show fracture surfaces at high magnification. There are many dimples of different sizes on the fracture surfaces, which display excellent plasticity [20]. Fig. 4(b, d, f) show that there are many small dimples around the large dimples, mainly because the large-sized precipitates form microvoids in the center of the dimples. When the microvoids grow to the appropriate size, the small-sized precipitated phase will also form microscopic voids, grow, and connect with the large voids, causing the inconsistent dimple size. Comparing Fig. 4(b, d, f), there are large secondary phase particles or inclusions present in the center of the dimples. Energy dispersive X-ray spectroscopy

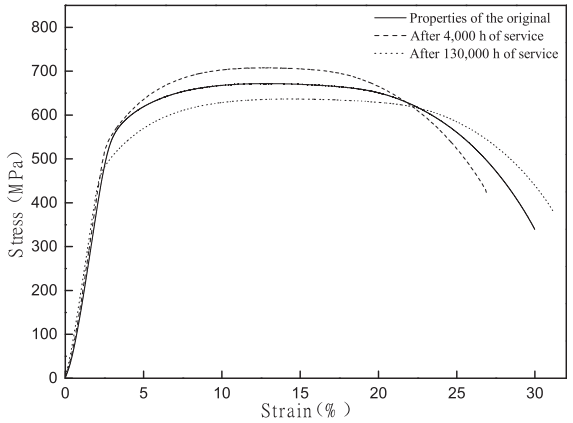

Fig. 3. Stress-strain curves of the T91 steel after different time in service.

(EDX) results show that the precipitates on the fracture surfaces are composed of Fe, Mo and Cr, Fe, C elements (Fig. 4g, h). Thus, it can be inferred that the type of precipitates is the Laves phase and $M_{23}C_6$ particles. The Laves phase formation, $M_{23}C_6$ coarsening, grain coarsening and laths widening usually lead to fracture [21,22]. Since binding of the secondary phase particles to the matrix is weak, under the tensile stress, the crack is first generated at the particle. This is the reason why the sample is most easily broken after 130,000 h of service, which is similar to the research results of Xia et al [12].

3.3. Scanning electron microscopy and energy spectra analysis

Fig. 5 compares the microstructure and properties of the T91 steel in its original state, and after 4000 h and 130,000 h of service. It can be seen by comparing Fig. 5(a, c, and e) that the precipitated phase in the original T91 steel is mainly located at the grain boundaries. The particle size of the precipitated phase increased from 0.44 μm in the original state and 0.42 μm after 4000 h in service to 0.94 μm after 130,000 h in service, and the precipitated phase aggregated and grew, which adversely affected the performance. The coarsening of $M_{23}C_6$ carbide may be due to the migration of solute atoms caused by dislocations motion. In addition, the rate of coarsening of the precipitated phase at the grain boundary is much larger than in the crystal, which is similar to the research results of Fujio et al. [23].

Fig. 5(b and d) show the chemical composition of the $M_{23}C_6$ carbide in T91 steel in the original state and after 4000 h of service, respectively. The chemical composition shows that the $M_{23}C_6$ carbide in the original T91 steel is mainly $Cr_{23}C_6$. After 4000 h of service, V in T91 steel will enter $M_{23}C_6$ to form Cr-rich multi-component mixed-phase $(Cr, Fe, V, Mo)_{23}C_6$, which will delay or inhibit the growth of the $M_{23}C_6$-type carbide during long-term high-temperature service, similar to Xu et al results [24]. Although the solid solution strengthening effect is weakened, the precipitation strengthening effect due to a large amount of precipitation phases is dominant, which is one of the reasons for the increase of material strength at this time period. After 130,000 h of service, the carbide coarsening is serious, and the alloying elements Cr, Nb, V, Mo or the like diffuse from the solid solution to the carbide. The depletion phenomenon of the solid solution alloy elements is severe, and the effect of solid solution strengthening is lowered, resulting in decreased hardness and strength.

The number of precipitated phase particles observed in the studied area and the percentage of the precipitated phase to the total area of the image are shown in Fig. 5(f). The percentage of carbides in T91 steel that has been in service for 4000 h has not changed much, but the number of carbide particles increased. The carbides are distributed along the grain boundaries, which can block the grain boundaries at high temperatures. Sliding and migration can increase the grain boundary strength. As the service time progresses, the T91 steel after 130,000 h in service is compared with the original T91 steel and in service for 4000 h, regardless of the amount of carbide. The percentage of the area is increased, the carbide coarsening is serious, and the coarsening of the carbide is prone to local stress concentration, which may cause the carbide to crack or separate from the matrix to generate voids or microcracks, and at the same time increase the space between carbide particles and decrease their volume fraction, degrading mechanical properties.

3.4. Transmission electron microscopy

In order to further study the effects of the type and size of the precipitated phase on material properties, the precipitated phase was studied and analyzed by transmission electron microscopy. Fig. 6 shows the TEM microstructure and precipitated phase diffraction spots of T91 steel after different service time. It is confirmed by diffraction analysis that the precipitated phases in T91 steel are mainly divided into $M_{23}C_6$-type carbide, MX-type carbide and the Laves phase. Previous studies have consistent results that the $M_{23}C_6$-type carbide is mainly distributed on the grain boundaries, while the MX-type carbide is mainly in the crystal, and the Laves phase is mainly at the grain boundaries or martensite lath bundles [25,26]. It was also reported that $Cr_{23}C_6$ is extremely unstable between 400 °C and 600 °C, which promotes embrittlement and sensitization of martensitic steels [27]. It can be seen from Fig. 6 that

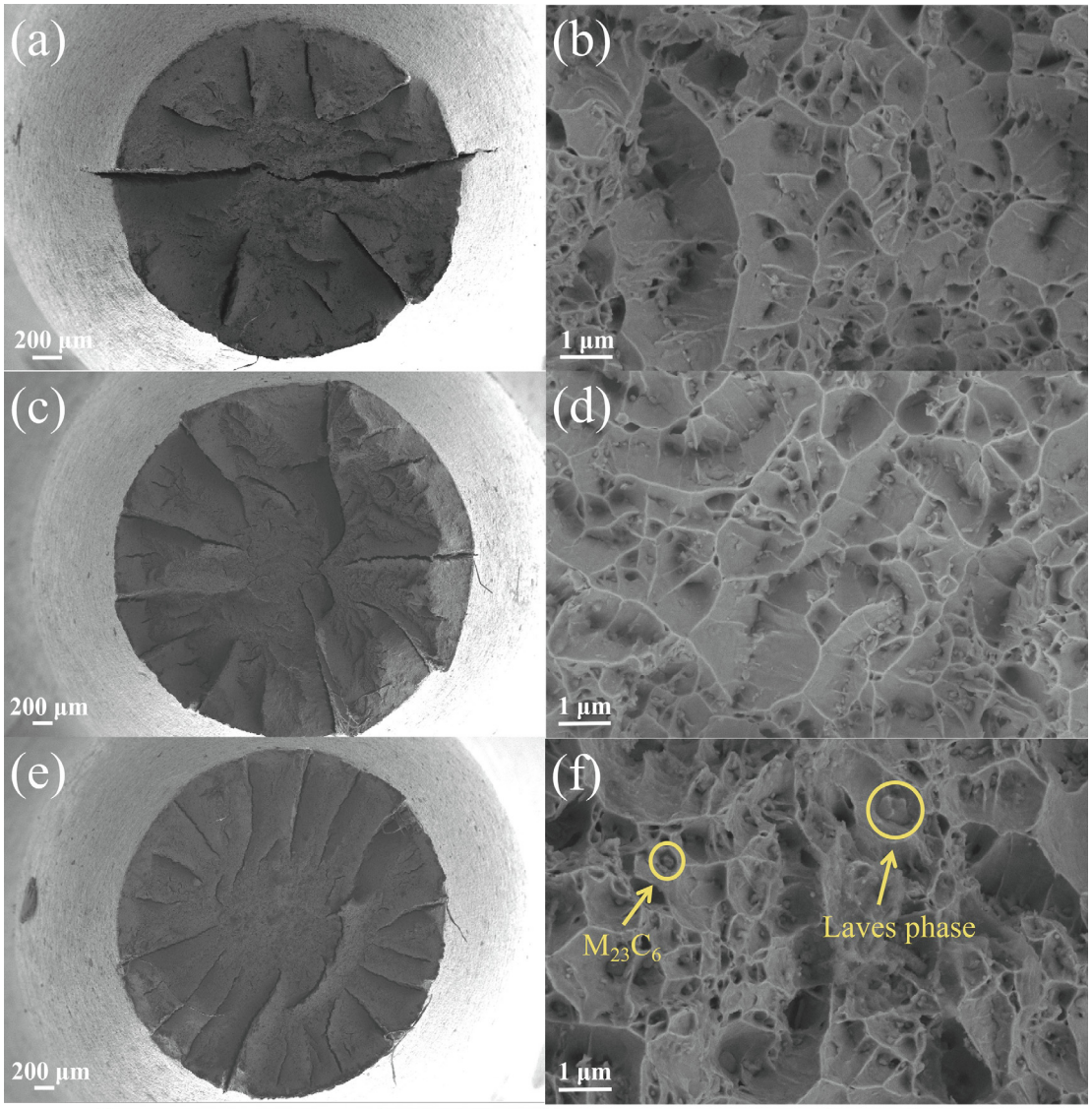

(g) Laves phase

Element	Wt.%
C	30.76
Fe	44.52
Cr	8.07
Mo	16.61
V	0.04

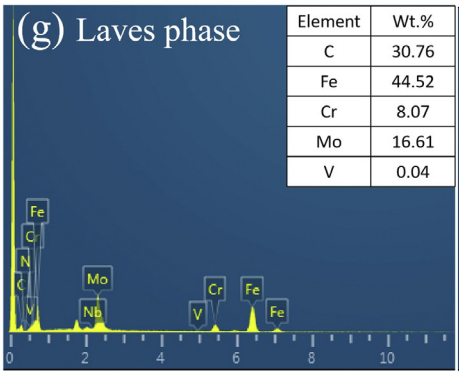

(h) $M_{23}C_6$

Element	Wt.%
C	41.24
Fe	31.95
Cr	24.37
Mo	1.87
V	0.48
Nb	0.09

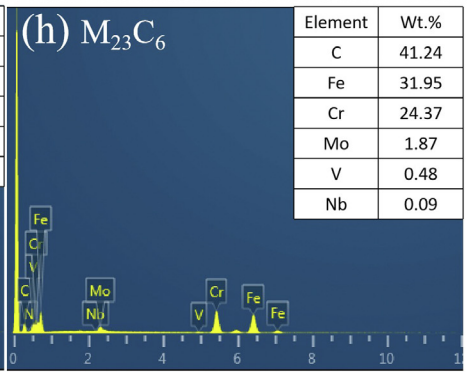

Fig. 4. SEM images of fracture surfaces obtained by tensile testing: (a) original at lower magnification, (b) original at higher magnification, (c) after 4000 h of service at lower magnification, (d) after 4000 h of service at higher magnification, (e) after 130,000 h of service at lower magnification, (f) after 130,000 h of service at higher magnification, (g) chemical composition of the Laves phase, (h) chemical composition of $M_{23}C_6$ carbide.

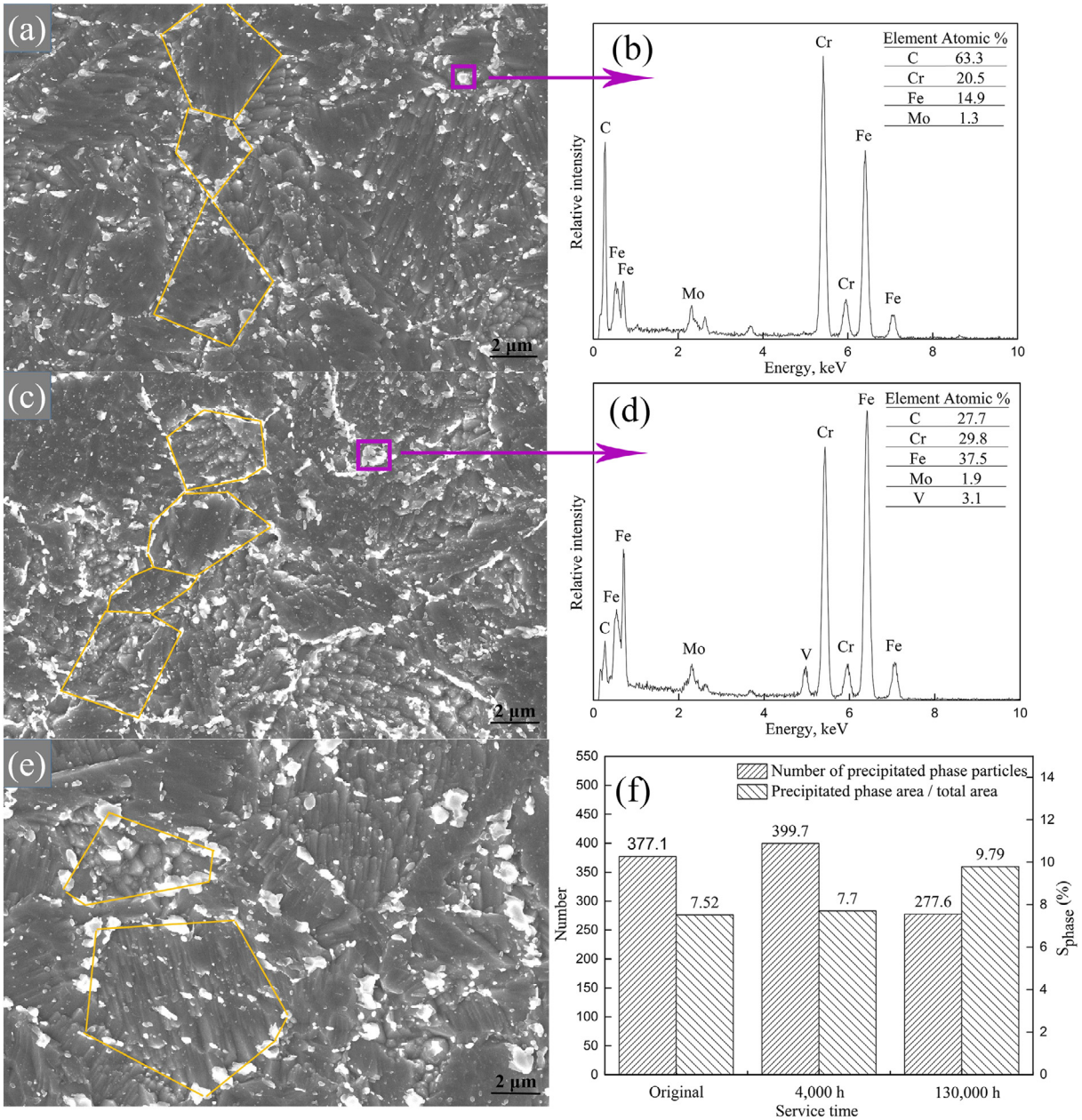

Fig. 5. SEM microstructure of the T91 steel from the Zhuhai power plant and statistical analysis of the EDS results of $M_{23}C_6$ carbide and precipitation phase: (a) original state, (b) original state, $M_{23}C_6$ carbide chemical composition, (c) 4000 h of service, (d) chemical composition of $M_{23}C_6$ carbide after 4000 h service, (e) 130,000 h of service, (f) statistical analysis of the number of precipitated phase particles and the percentage of precipitated phase area to the total area.

the original state in Fig. 6(a) is mainly martensite lath, with some dislocations and many $M_{23}C_6$ particles at the lath. Besides, there are fine MC-type carbides inside. In Fig. 6(b) martensite lath slats exhibit a small number of subgrains, which have a high dislocation density in the martensite lath, which is distributed on the carbides, hindering the migration of dislocations, leading to dislocation strengthening [28]. Dislocations entanglement into a dislocation network, stronger interactions between dislocations and the solid solution atoms, carbides, and subgrains, strengthened the matrix. MX-type carbides pin dislocations in the crystal. The dislocations bypass or pass through the carbides, requiring additional energy and hindering the recovery. Therefore, the material's strength is higher. After 130,000 h of service, martensite begins to shatter and widen, the subgrain structure increases, the dislocation density decreases, and the precipitated phase coarsening reduces the pinning of carbides, which promotes the growth of subgrains [29]. Panait et al. [30] found that creep damage was observed near the Laves phase, which means that the loss of creep strength is probably due to the coarsened Laves phases and significant recovery of the matrix. Pandey et al. [31] studied the formation of Laves phase and

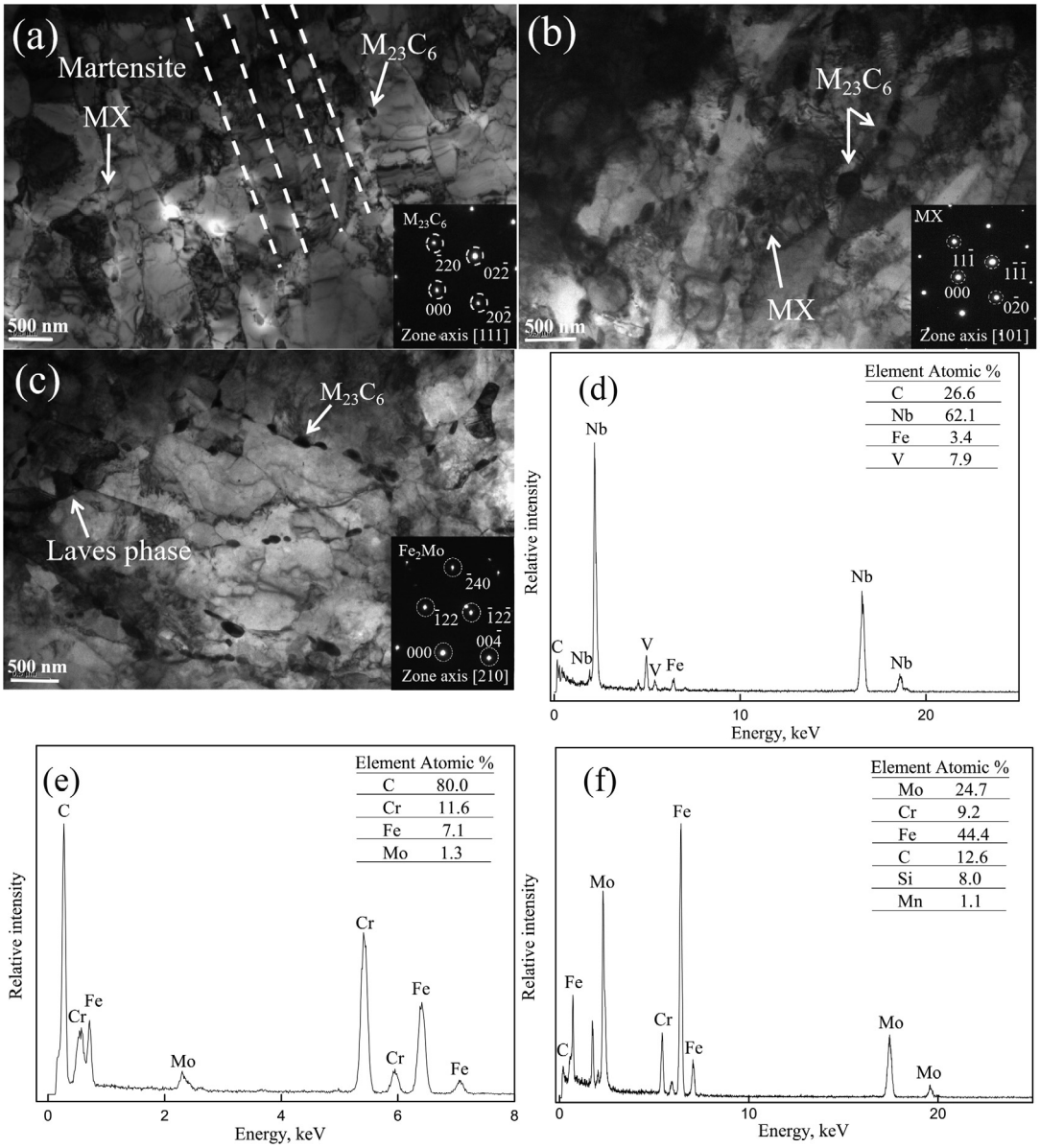

Fig. 6. TEM microstructure of T91 steel from the Zhuhai power plant: (a) original state, and the diffraction spot is $M_{23}C_6$ in the figure, (b) after 4000 h of service, and the diffraction spot is MX in the figure, (c) after 130,000 h of service, and the diffraction spot is the Laves phase in the figure, (d) original state, MX carbide chemical composition, (e) chemical composition of $M_{23}C_6$ carbide after 4000 h service, (f) chemical composition of Laves phase after 130,000 h service.

the reduction of precipitate density at 620 °C for 120 MPa stress, which led to the failure of P91 steel. This means that the loss of strength is probably mainly due to coarsening of $M_{23}C_6$ carbides, significant precipitation and coarsening of the Laves phases and significant recovery of the matrix. The Laves phase (Fe_2Mo) formed in the sample when the T91 steel was in service between 4000 h and 130,000 h. As the service time increases, the growth of the Laves phase causes Mo to diffuse from the solid solution to the precipitation phase. The study shows that the $M_{23}C_6$ is coarse. The agglomeration of the Laves phase results in degraded mechanical properties of the material [32]. Two mechanisms of the nucleation and growth of the Laves phase have been described [33,34]. One mechanism claims that the nucleation of Laves phase occurs on martensite lath boundaries or subgrain boundaries without the presence of $M_{23}C_6$ carbide. The other nucleation mechanism considers that the Laves phase precipitates in Cr-depleted regions adjacent to $M_{23}C_6$ particles. For the case of the studied T91 steels both of the two mechanisms are responsible for the formation of the Laves phases.

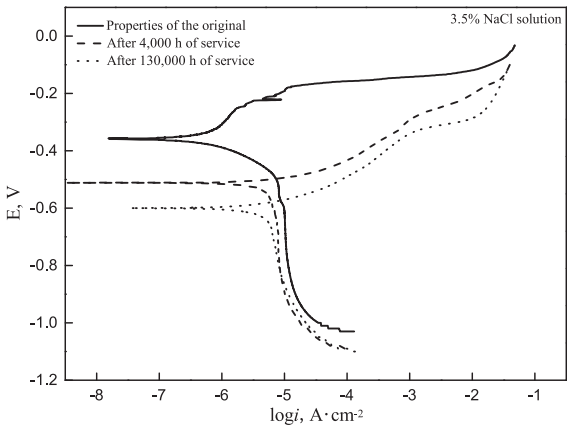

Fig. 7. Polarization curves of T91 steel with different service time in 3.5% NaCl solution.

Table 2
The corrosion potential, corrosion current density, corrosion rate of the T91 steel after different service time.

Corrosive medium	T91	Corrosion potential, V	Corrosion current density, A/cm^2	Corrosion rate, mm/a
3.5 wt% NaCl	Original	−0.358	7.454×10^{-7}	0.0088
3.5 wt% NaCl	4000 h	−0.512	1.891×10^{-6}	0.022
3.5 wt% NaCl	130,000 h	−0.6	3.517×10^{-6}	0.041

3.5. Electrochemical tests

Fig. 7 shows the potentiodynamic polarization curves of the T91 steel in 3.5 wt% NaCl solution after different service time. Table 2 illustrates the correlation results of corrosion potential, corrosion current density and corrosion rate obtained from the polarization curves. As the service time increases, the corrosion potential decreases, while the corrosion current density, and the corrosion rate increase, and the corrosion resistance decreases. At the same time, between 4000 h and 130,000 h of service, the increase of the corrosion current density of the sample is greater than from the original state to 4000 h of service. According to the Faraday's second law, there is a relationship between the corrosion current density and the corrosion rate [35]. The greater the corrosion current density, the greater the corrosion rate [35], so the corrosion rate during the 4000–130,000 h service period is greater than from the original period to 4000 h. This is because the precipitation phase is severely coarsened between 4000 h and 130,000 h of service, the alloying elements solid solution is depleted, and the degree of segregation of Cr and Mo elements is deepened, resulting in a decrease in corrosion resistance of the material. In general, the corrosion resistance of the T91 steel in 3.5% wt. NaCl solution decreased with service time.

4. Conclusions

The paper focused on the evolution of microstructure and mechanical properties of T91 steel after long service time up to 130,000 h in an actual power plant. The following conclusions are drawn from the study:

(1) After 4000 h of service, V in T91 steel will enter $M_{23}C_6$ to form Cr-rich multi-component mixed-phase $(Cr, Fe, V, Mo)_{23}C_6$, which will delay or inhibit the growth of the $M_{23}C_6$-type carbide during long-term high-temperature service. After 130,000 h of service, the martensite begins to shatter and widen, and the dislocation density decreases. In addition, the Laves phase (Fe_2Mo) formed in the sample.
(2) The percentage of carbides in T91 steel didn't change too much after 4000 h service, but the number of carbide particles increased. As the service time progressed, the number and the percentage of carbides in T91 steel increased and coarsened.
(3) The hardness and strength of T91 steel initially increased and then decreased during long-term service.
(4) With longer service time, the depletion of Cr and Mo elements became more severe, and the ability of T91 steel to resist corrosion decreased.

Declaration of Competing Interest

No conflict of interest exits in the submission of this manuscript, and manuscript is approved by all authors for publication.

Acknowledgments

This work was supported by the Shenhua Guohua (Beijing) Electric Power Research Institute Co., Ltd. Xiaolu Pang acknowledges support from the National Natural Science Foundation of China (No. 51922002).

References

[1] J. Hald, Creep strength and ductility of 9 to 12% chromium steels, Mater. High Temp. 21 (1) (2004) 41–46, https://doi.org/10.1179/mht.2004.006.
[2] W. Bendick, L. Cipolla, J. Gabrel, J. Hald, New ECCC assessment of creep rupture strength for steel grade X10CrMoVNb9-1 (Grade 91), Int. J. Press. Vessels Pip. 87 (6) (2010) 304–309, https://doi.org/10.1016/j.ijpvp.2010.03.010.
[3] A. Czyrska-Filemonowicz, A. Zielińska-Lipiec, P.J. Ennis, Modified 9% Cr steels for advanced power generation: microstructure and properties, J. Achiev. Mater. Manuf. Eng. 19 (2) (2006) 43–48.
[4] T. Ogata, T. Sakai, M. Yaguchi, Damage assessment method of P91 steel welded tube under internal pressure creep based on void growth simulation, Int. J. Pres. Ves. Pip. 87 (11) (2010) 611–616, https://doi.org/10.1016/j.ijpvp.2010.08.009.
[5] M.Z. Hamzah, W.H. Yeo, A.T. Fry, J.I. Inayat-Hussain, S. Ramesh, J. Purbolaksono, Estimation of oxide scale growth and temperature increase of high (9–12%) chromium martensitic steels of superheater tubes, Eng. Fail. Anal. 35 (2013) 380–386, https://doi.org/10.1016/j.engfailanal.2013.03.014.
[6] S. Fetni, W. Jhinaoui, C. Boubahri, D. Montero, J. Briki, Analysis of changes in lattice parameter of a grade 91 steel during thermal ageing at 550 °C, Eng. Fail. Anal. 97 (2019) 43–52, https://doi.org/10.1016/j.engfailanal.2018.12.006.
[7] Z. Shang, J. Ding, C. Fan, M. Song, J. Li, Q. Li, S. Xue, K.T. Hartwig, X. Zhang, Tailoring the strength and ductility of T91 steel by partial tempering treatment, Acta Mater. 169 (2019) 209–224, https://doi.org/10.1016/j.actamat.2019.02.043.
[8] T. Olszewski, Oxidation Mechanisms of Materials for Heat Exchanging Components in CO_2/H_2O-Containing Gases Relevant to Oxy-fuel Environments, Forschungszentrum Jülich GmbH, Jülich, Germany, 2012.
[9] A. Shibli, F. Starr, Some aspects of plant and research experience in the use of new high strength martensitic steel P91, Int. J. Pres. Ves. Pip. 84 (1–2) (2007) 114–122, https://doi.org/10.1016/j.ijpvp.2006.11.002.
[10] H. Li, D. Mitchell, Microstructural characterization of P91 steel in the virgin, service exposed and post-service re-normalized conditions, Steel Res. Int. 84 (12) (2013) 1302–1308, https://doi.org/10.1002/srin.201300055.
[11] J. Parker, In-service behavior of creep strength enhanced ferritic steels Grade 91 and Grade 92–Part 1 parent metal, Int. J. Pres. Ves. Pip. 101 (2013) 30–36, https://doi.org/10.1016/j.ijpvp.2012.10.001.
[12] Z.X. Xia, C.Y. Wang, Y.F. Zhao, G.D. Zhang, L. Zhang, X.M. Meng, Laves phase formation and its effect on mechanical properties in P91 steel, Acta Metall. Sin. (Engl. Lett.) 28 (10) (2015) 1238–1246, https://doi.org/10.1007/s40195-015-0318-5.
[13] A. Baltušnikas, A. Grybėnas, R. Kriūkienė, I. Lukošiūtė, V. Makarevičius, Evolution of crystallographic structure of $M_{23}C_6$ carbide under thermal aging of P91 steel, J. Mater. Eng. Perform. 28 (3) (2019) 1480–1490, https://doi.org/10.1007/s11665-019-03935-1.
[14] J. Blach, L. Falat, P. Ševc, Fracture characteristics of thermally exposed 9Cr–1Mo steel after tensile and impact testing at room temperature, Eng. Fail. Anal. 16 (5) (2009) 1397–1403, https://doi.org/10.1016/j.engfailanal.2008.09.003.
[15] F. Kafexhiu, F. Vodopivec, J.V. Turna, Effect of tempering on the room-temperature mechanical properties of X20CrMoV121 and P91 steels, Mater. Technol. 46 (5) (2012) 459–464.
[16] C. Pandey, M.M. Mahapatra, Effect of long-term ageing on the microstructure and mechanical properties of creep strength enhanced ferritic P91 steel, Trans. Indian Inst. Met. 69 (9) (2016) 1657–1673, https://doi.org/10.1007/s12666-015-0826-z.
[17] C. Pandey, Effect of heat treatment on mechanical behavior and microstructure feature of the thermal aged P91 steel, Mater. Res. Express 6 (9) (2019) 096541, , https://doi.org/10.1088/2053-1591/ab2e5e.
[18] ASTM International, ASTM A213/A213M-06a: Standard Specification for Seamless Ferritic and Austenitic Alloy-Steel Boiler, Superheater, and Heat-Exchanger Tubes, ASTM International, West Conshohocken, PA, 2006.
[19] C. Pandey, A. Giri, M.M. Mahapatra, P. Kumar, Characterization of microstructure of HAZs in as-welded and service condition of P91 pipe weldments, Met. Mater. Int. 23 (1) (2017) 148–162, https://doi.org/10.1007/s12540-017-6394-5.
[20] J. Cao, Y. Gong, K. Zhu, Z.G. Yang, X.M. Luo, F.M. Gu, Microstructure and mechanical properties of dissimilar materials joints between T92 martensitic and S304H austenitic steels, Mater. Des. 32 (5) (2011) 2763–2770, https://doi.org/10.1016/j.matdes.2011.01.008.
[21] C. Pandey, N. Saini, M.M. Mahapatra, P. Kumar, Study of the fracture surface morphology of impact and tensile tested cast and forged (C&F) Grade 91 steel at room temperature for different heat treatment regimes, Eng. Fail. Anal. 71 (2017) 131–147, https://doi.org/10.1016/j.engfailanal.2016.06.012.
[22] C. Pandey, M.M. Mahapatra, P. Kumar, S. Sirohi, Fracture behaviour of crept P91 welded sample for different post weld heat treatments condition, Eng. Fail. Anal. 95 (2019) 18–29, https://doi.org/10.1016/j.engfailanal.2018.08.029.
[23] F. Abe, T. Horiuchi, K. Sawada, High-temperature annealing for maximization of dissolved boron in creep-resistant martensitic 9Cr steel, Mater. Sci. Forum 426–432 (2003) 1393–1398, https://doi.org/10.4028/www.scientific.net/MSF.426-432.1393.
[24] Y. Xu, X. Zhang, Y. Tian, C. Chen, Y. Nan, H. He, M. Wang, Study on the nucleation and growth of $M_{23}C_6$ carbides in a 10% Cr martensite ferritic steel after long-term aging, Mater. Charact. 111 (2016) 122–127, https://doi.org/10.1016/j.matchar.2015.11.023.
[25] J. Hald, Microstructure and long-term creep properties of 9–12% Cr steels, Int. J. Pres. Ves. Pip. 85 (1–2) (2008) 30–37, https://doi.org/10.1016/j.ijpvp.2007.06.010.
[26] Z.F. Peng, S. Liu, C. Yang, F.Y. Chen, F.F. Peng, The effect of phase parameter variation on hardness of P91 components after service exposures at 530–550°C, Acta Mater. 143 (2018) 141–155, https://doi.org/10.1016/j.actamat.2017.10.010.
[27] S.S.M. Tavares, F.J. Da Silva, C. Scandian, G.F. Da Silva, H.F.G. De Abreu, Microstructure and intergranular corrosion resistance of UNS S17400 (17–4PH) stainless steel, Corros. Sci. 52 (11) (2010) 3835–3839, https://doi.org/10.1016/j.corsci.2010.07.016.
[28] V.K. Sikka, Development of modified 9Cr-1Mo for elevated-temperature service, in: J.W. Davis, D.J. Michel (Eds.), ProcTop. Conf. on Ferritic Alloys for Use in Nuclear Energy Technologies, The Metallurgical Society, Warrendale, PA, 1983, pp. 55–74.
[29] H. Ghassemi-Armaki, R.P. Chen, K. Maruyama, M. Yoshizawa, M. Igarashi, Static recovery of tempered lath martensite microstructures during long-term aging in 9–12% Cr heat resistant steels, Mater. Lett. 63 (28) (2009) 2423–2425, https://doi.org/10.1016/j.matlet.2009.08.024.
[30] C.G. Panait, W. Bendick, A. Fuchsmann, A.F. Gourgues-Lorenzon, J. Besson, Study of the microstructure of the Grade 91 steel after more than 100,000 h of creep exposure at 600 °C, Int. J. Pressure Vessels Piping 87 (6) (2010) 326–335, https://doi.org/10.1016/j.ijpvp.2010.03.017.
[31] C. Pandey, M.M. Mahapatra, P. Kumar, R.S. Vidyrathy, A. Srivastava, Microstructure-based assessment of creep rupture behaviour of cast-forged P91 steel, Mater. Sci. Eng. A 695 (2017) 291–301, https://doi.org/10.1016/j.msea.2017.04.037.
[32] S. Fetni, A. Toumi, I. Mkaouar, C. Boubahri, J. Briki, Microstructure evolution and corrosion behaviour of an ASTM A213 T91 tube after long term creep exposure, Eng. Fail. Anal. 79 (2017) 575–591, https://doi.org/10.1016/j.engfailanal.2017.03.023.
[33] Y. Tsuchida, K. Okamoto, Y. Tokunaga, Improvement of creep rupture strength of high Cr ferritic steel by addition of W, ISIJ Int. 35 (3) (1995) 317–323, https://doi.org/10.2355/isijinternational.35.317.
[34] P.J. Ennis, A. Czyrska-Filemonowicz, Recent advances in creep-resistant steels for power plant applications, Sadhana 28 (3–4) (2003) 709–730, https://doi.org/10.1007/BF02706455.
[35] T. Ohtsuka, T. Komatsu, Enhancement of electric conductivity of the rust layer by adsorption of water, Corros. Sci. 47 (10) (2005) 2571–2577, https://doi.org/10.1016/j.corsci.2004.10.010.